

Enhanced cyclability of Li–O₂ batteries with cathodes of Ir and MnO₂ supported on well-defined TiN arrays

Limin Leng,^{ab} Jing Li,^a Xiaoyuan Zeng,^a Xinlong Tian,^a Huiyu Song,^a Zhimin Cui,^{*a} Ting Shu,^a Haishui Wang,^a Jianwei Ren^c and Shijun Liao^{*a}

Author affiliations

* Corresponding authors

^a The Key Laboratory of Fuel Cell Technology of Guangdong Province, School of Chemistry and Chemical Engineering, South China University of Technology, Guangzhou 510641, China

E-mail: cuizm26@gmail.com, chsjliao@scut.edu.cn

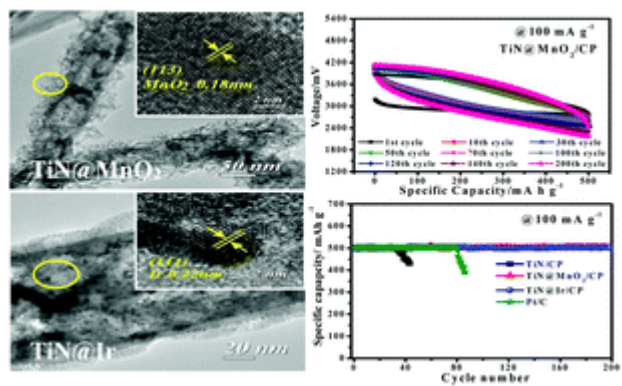
Fax: +86 20 87113586

^b Sunwoda Electronic Co., Ltd, Shenzhen, China

^c HySA Infrastructure Centre of Competence, Materials Science and Manufacturing, Council for Scientific and Industrial Research (CSIR), PO Box 395, Pretoria 0001, South Africa

Abstract

The cycling stability of Li–O₂ batteries has been impeded by the lack of high-efficiency, and durable oxygen cathodes for the oxygen-reduction reaction (ORR) and the oxygen-evolution reaction (OER). Herein we report a novel TiN nanorod array-based cathode, which was firstly prepared by growing a TiN nanorod array on carbon paper (CP), and then followed by depositing MnO₂ ultrathin sheets or Ir nanoparticles on the TiN nanorods to form well-ordered, three-dimensional (3D), and free-standing structured cathodes: TiN@MnO₂/CP and TiN@Ir/CP. Both cathodes exhibited good specific capacity and excellent cycling stability. Their specific discharge capacities were up to 2637 and 2530 mA h g⁻¹, respectively. After 200 cycles for 2000 h at a current density of 100 mA g⁻¹, no obvious decays were observed for TiN@MnO₂/CP and TiN@Ir/CP cathodes, while significant decreases were observed after the 80th and 30th cycles for the Pt/C and TiN/CP cathodes, respectively. Such high performance can be ascribed to the 3D array structure with enough microspace and high surface area, which facilitated the high dispersion of active components and prevented the formation of large/irreversible Li₂O₂.



Supporting Information

Enhanced cyclability of Li-O₂ battery with cathodes of Ir and MnO₂ supported on well defined TiN array

*Limin Leng ^{a,b}, Jing Li ^a, Xiaoyuan Zeng ^a, Xinlong Tian ^a, Huiyu Song ^a,
Zhiming Cui ^{a,*}, Ting Shu ^a, Haishui Wang ^a, Jianwei Ren ^c, Shijun Liao ^{a,*}*

^a*The Key Laboratory of Fuel Cell Technology of Guangdong Province, School of Chemistry
and Chemical Engineering, South China University of Technology, Guangzhou 510641,
China.*

^b*Sunwoda Electronic Co., Ltd, Shenzhen, Guangdong 518100, China*

^c*HySA Infrastructure Centre of Competence, Materials Science and Manufacturing, Council
for Scientific and Industrial Research (CSIR). PO Box 395, Pretoria 0001, South Africa.*

* Corresponding author Fax: +86 20 87113586. E-mail address: chsjliao@scut.edu.cn
* Corresponding author Fax: +86 20 87113586. E-mail address: cuizm26@gmail.com

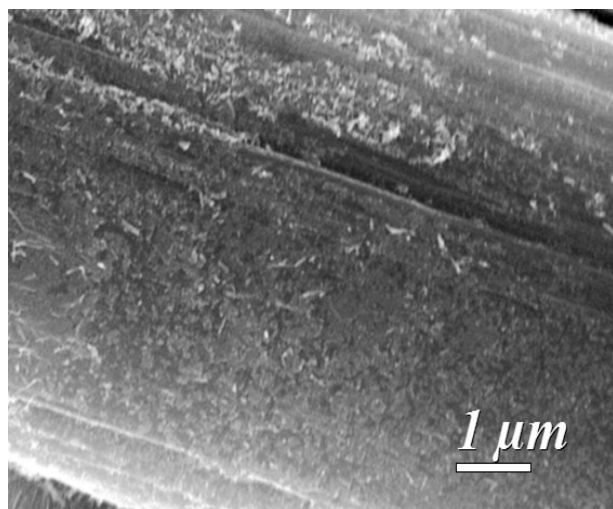


Fig. S1 SEM image of the sample after seed layer is generated on the carbon paper.

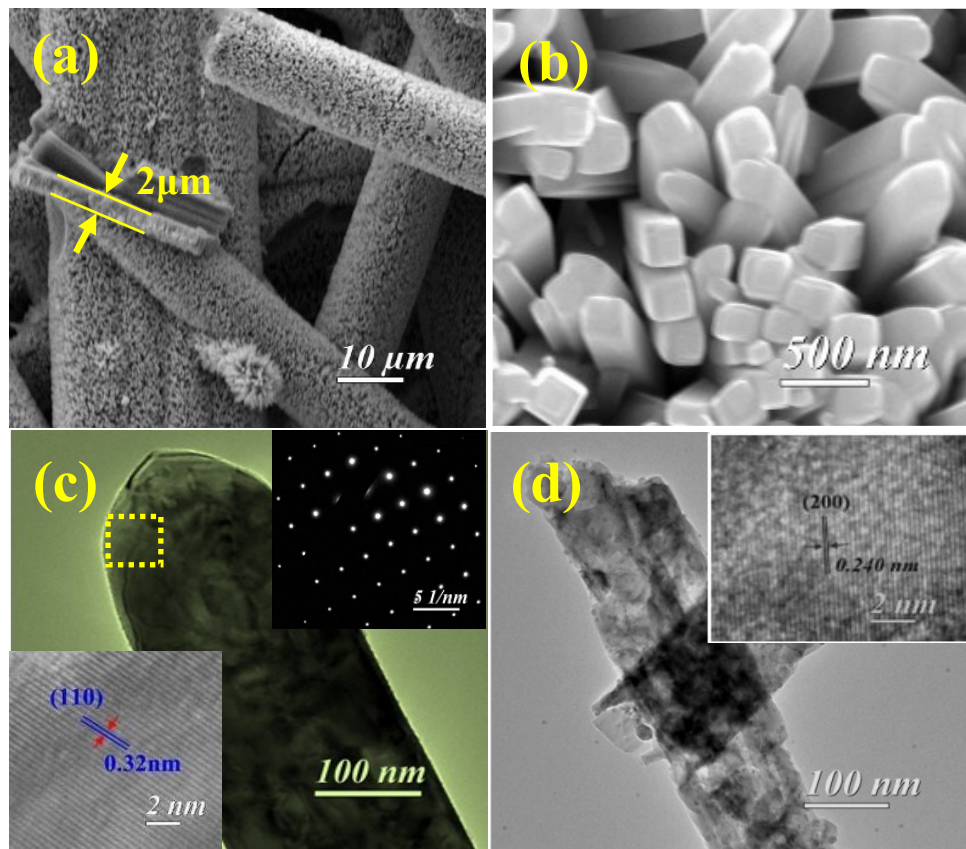


Fig. S2 SEM and magnified SEM images of (a, b) TiO_2/CP ; TEM images of (c) TiO_2 nanorod, and (d) TiN nanorod catalysts (the insets are the SAED pattern and HR-TEM images).

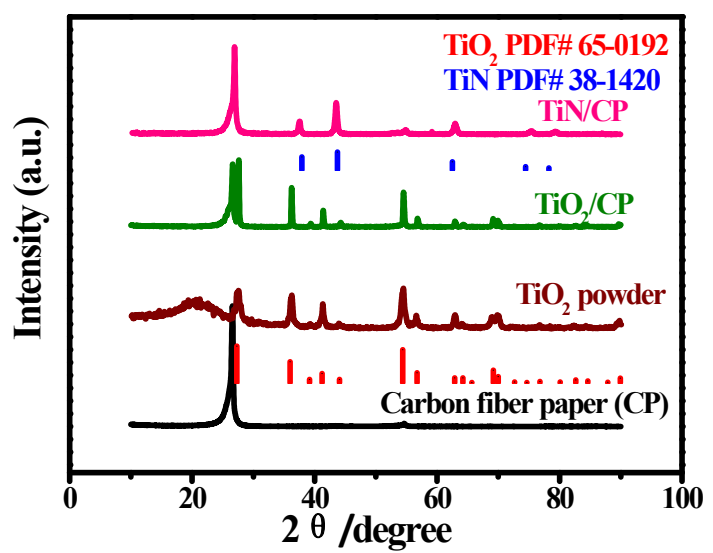


Fig. S3 XRD patterns of the as-prepared various cathodes.

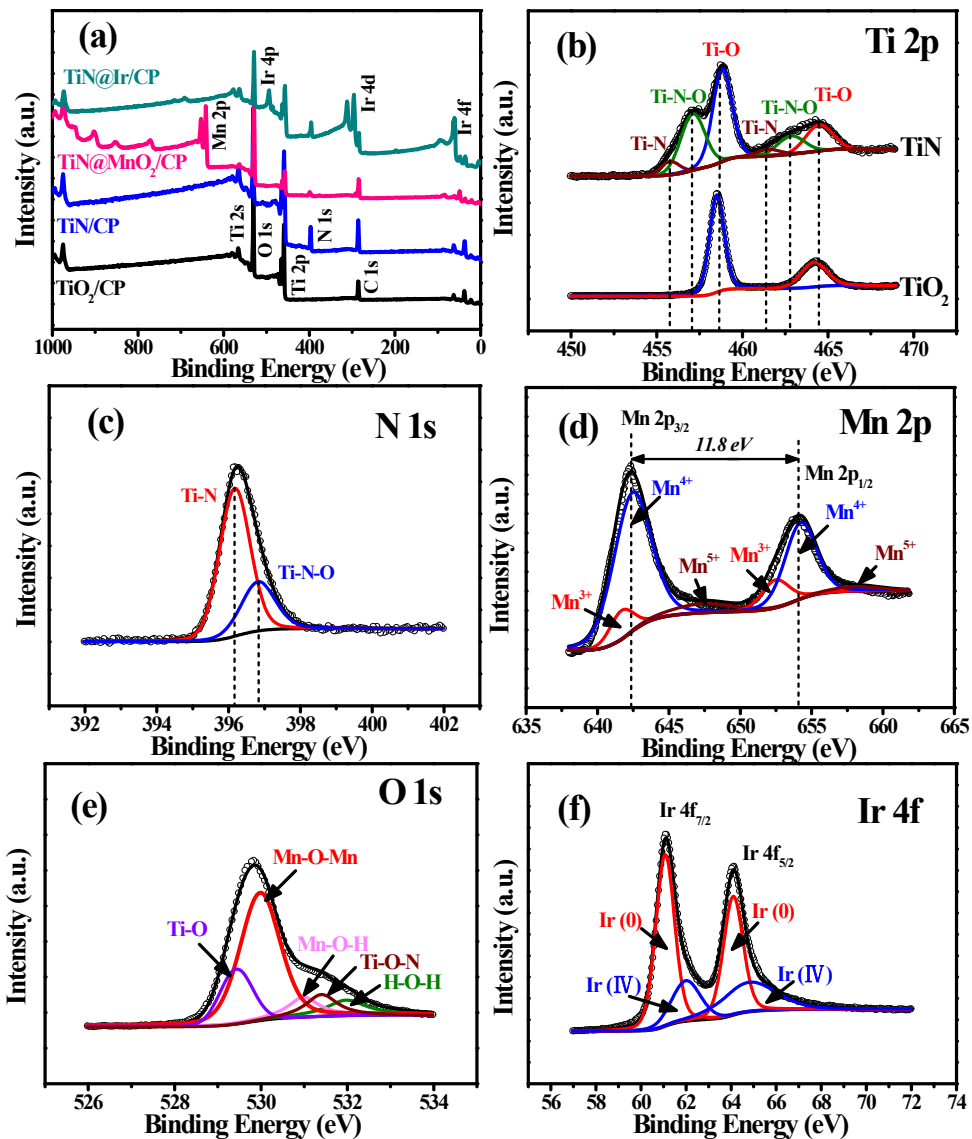


Fig. S4 XPS spectrum of (a) the as-prepared electrodes and b) Ti 2p, (c) N1s, (d) Mn 2p, (e) O 1s and (f) Ir 4f.

The XPS survey spectra of TiN/CP cathode exhibits the N 1s peak with a bond energy around 396 eV (Figure S3c), confirming the N substituting O atom in the crystal lattice and formation of the Ti–N. Multiple peaks are evolved at lower binding energies in the Ti 2p spectra as depicted in Fig. S3b, which can be assigned to be Ti–N ($2p_{3/2} = 455.8$ eV and $2p_{1/2} = 461.53$ eV), Ti–N–O ($2p_{3/2} = 457.12$ eV and $2p_{1/2} = 463.1$ eV), and Ti–O ($2p_{3/2} = 458.84$ eV and $2p_{1/2} = 464.5$ eV)¹⁻³. Moreover, N 1s spectrum (Fig. S3c) was analyzed by deconvolution method, the characteristic peaks at binding energies of 396.18 and 396.83 eV correspond to Ti–N and Ti–N–O peaks,

respectively. Fig. S4d and e display the Mn 2p and O1s spectra for the TiN@MnO₂/CP cathode, respectively. The Mn 2p spectrum presents two main peaks located at 642.45 and 654.25 eV, being assigned to Mn 2p_{3/2} and Mn 2p_{1/2} with a spin-energy separation of 11.8 eV, which are in accordance with the previous reports on MnO₂^{4, 5}. In the O 1s region, there are three peaks with the binding energies of 529.8, 531.0 and 532.0 eV. The sharp peak located at 529.8 eV is for O element in Mn–O–Mn oxide, and other two peaks at 531.0 and 532.0 eV correspond to O element in hydroxide (Mn–O–H) and water (H–O–H)^{4, 6}. The high resolution XPS spectrum of Ir 4f (Fig. S3f) exhibits dominating Ir (0) 4f_{5/2} and Ir (0) 4f_{7/2} with fractional Ir (IV) 4f_{5/2} and Ir (IV) 4f_{7/2} suggesting a certain degree of surface oxidation, which is a common phenomenon among metal nanoparticles.

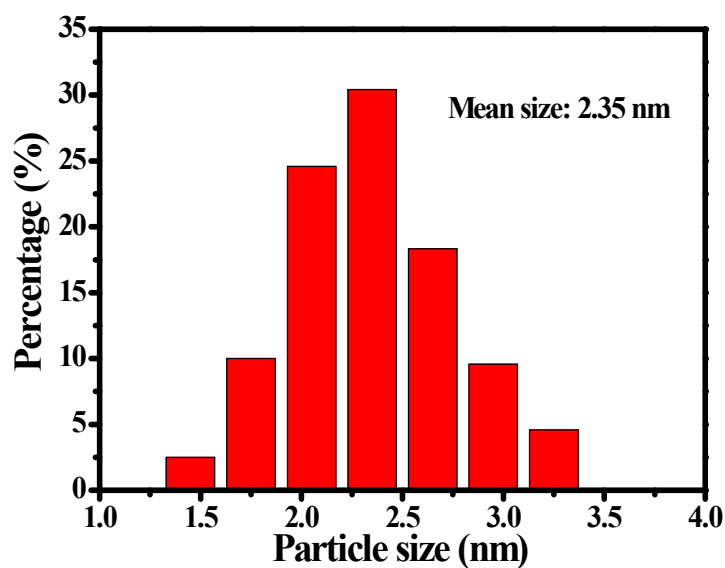


Fig. S5 The particle size distribution of iridium nanoparticles in TiN@Ir catalyst.

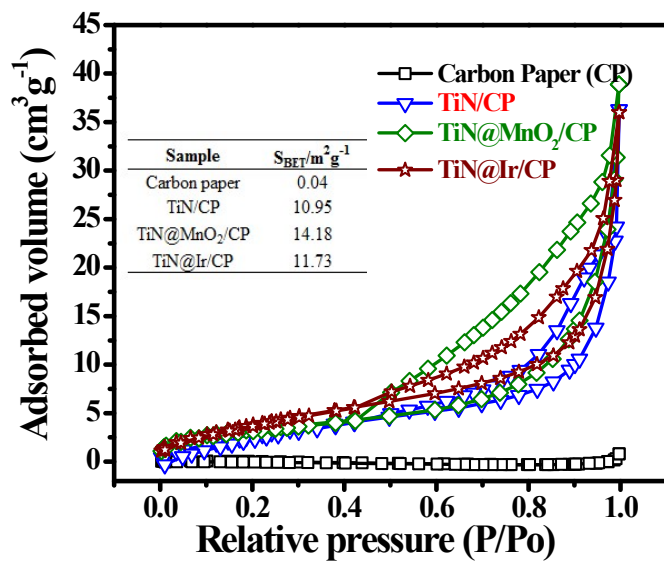


Fig. S6 N₂ adsorption-desorption isotherms of various cathodes.

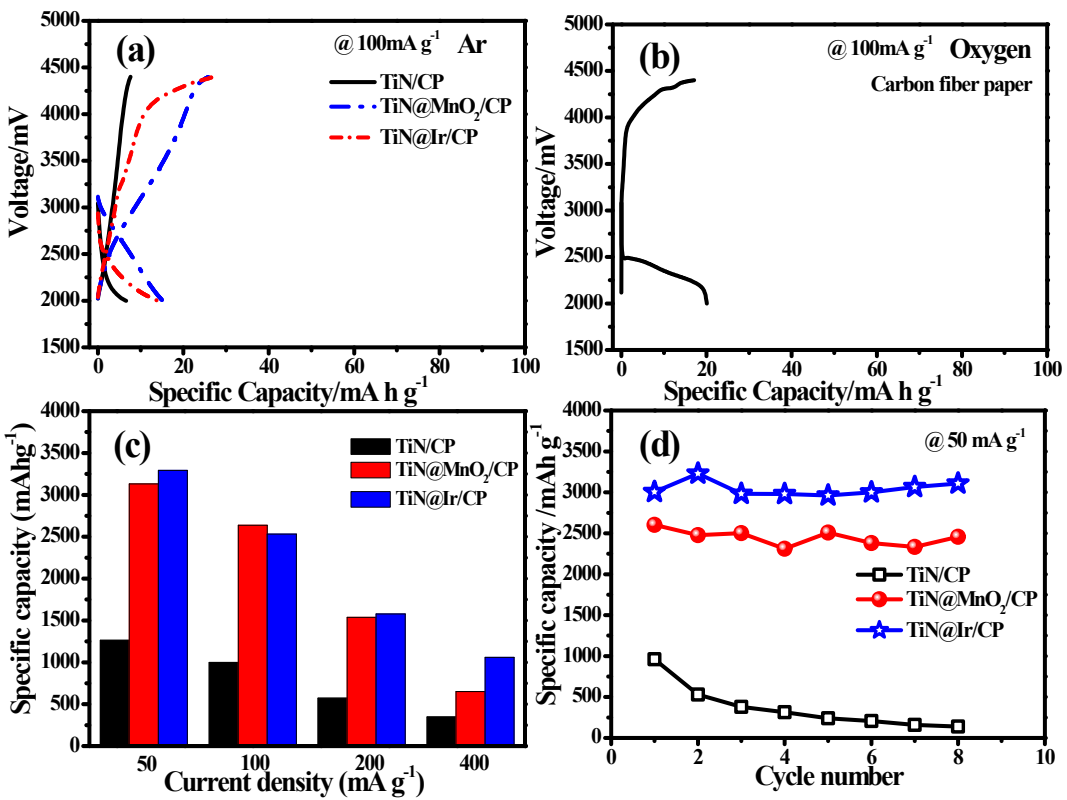


Fig. S7 The discharge-charge curves of the various electrodes at 100 mA g^{-1} under (a) Ar and (b) O₂ atmosphere; (c) Specific capacities and (d) cycling performance of Li–O₂ batteries with various cathodes.

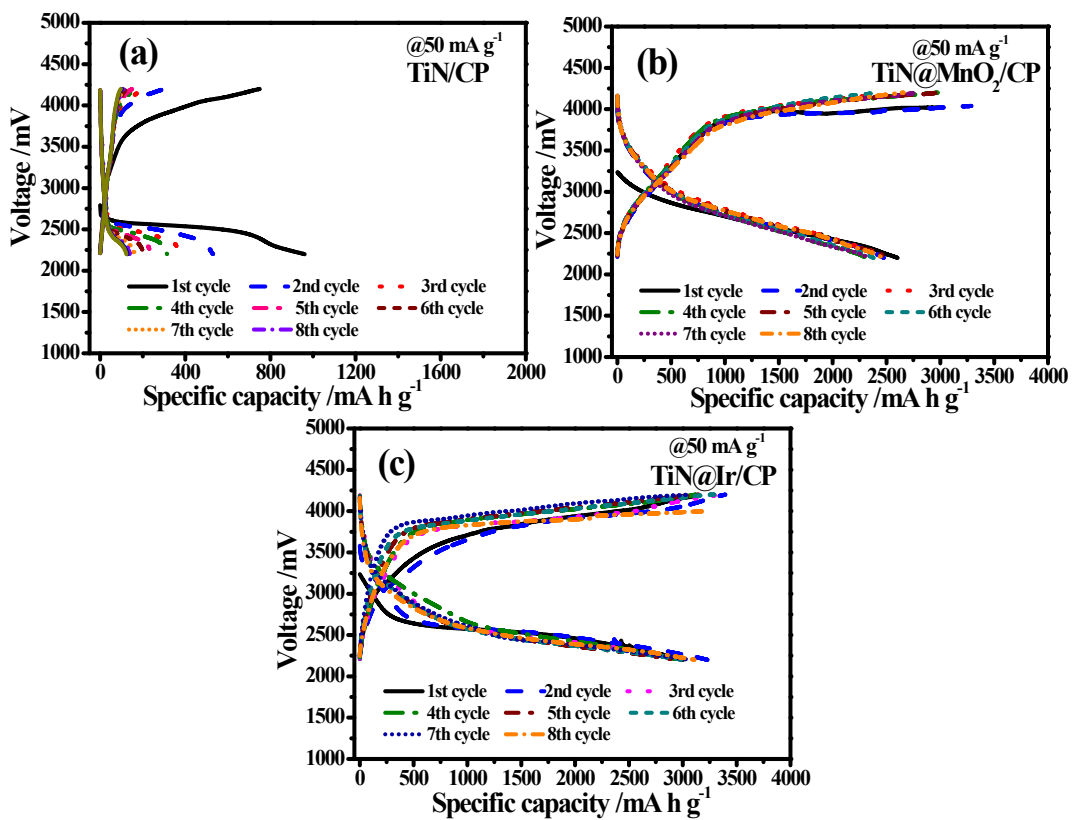


Fig. S8 Discharge/charge curves of Li–O₂ batteries with (a) TiN/CP, (b) TiN@MnO₂/CP and (c) TiN@Ir/CP cathodes at 50 mA g⁻¹.

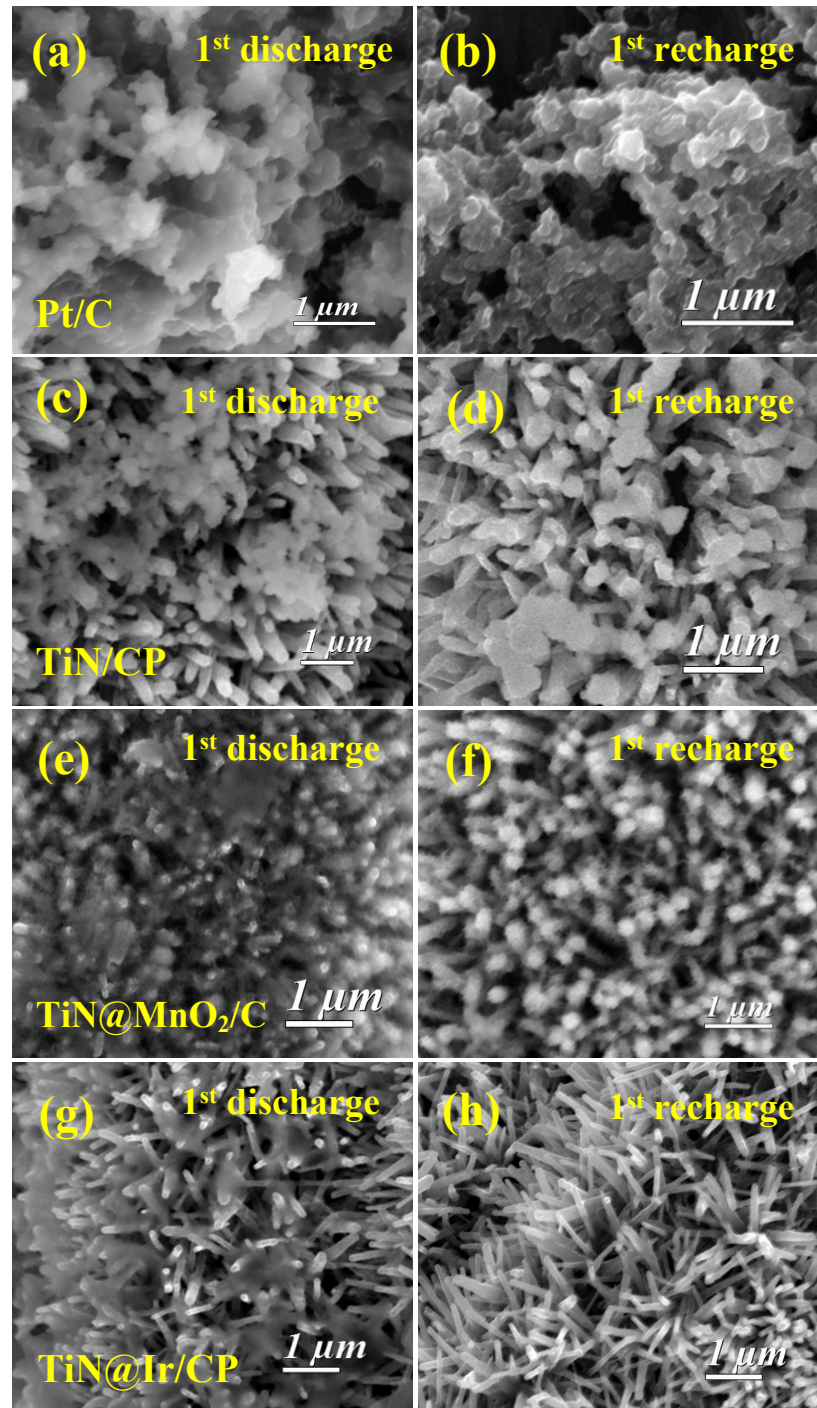


Fig. S9 SEM images of (a, b) Pt/C; (c, d) TiN/CP; (e, f) TiN@MnO₂/CP and (g, h) TiN@Ir/CP cathodes after the first fully discharged (a, c, e, g) and recharged (b, d, f, h) process at a current density of 100 mA g⁻¹.

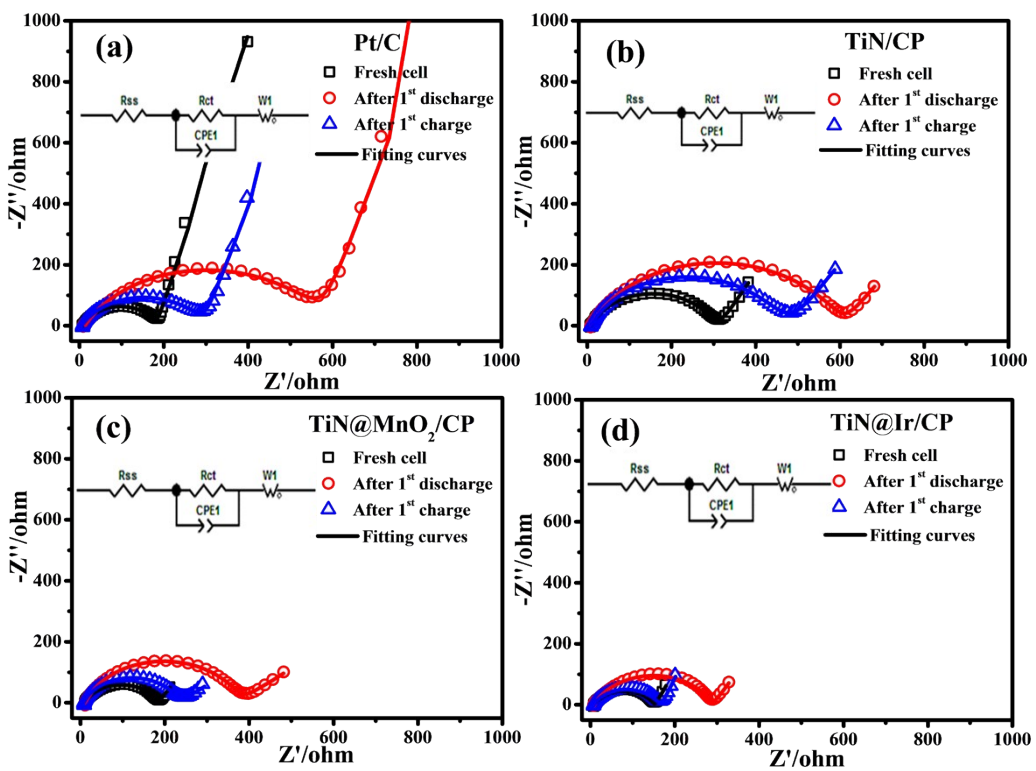


Fig. S10 Electrochemical impedance spectra (EIS) of Li–O₂ batteries with various cathodes (a) Pt/C, (b) TiN/CP, (c) TiN@MnO₂/CP and (d) TiN@Ir/CP at the first fully discharged and recharged.

Table S1 Values of the fitting parameters evaluated from the equivalent circuit with various cathodes at the first fully discharged/charged.

Catalytic cathodes	State	Rss /ohm	Rct /ohm	CPE-T /μF	CPE-P	W1-R /ohm	W1-T /F	W1-P
Pt/C	Fresh	10.01	173.5	10.87	0.80	5694	14.24	0.85
	discharged	12.75	564.7	16.96	0.72	7328	16.54	0.84
	recharged	9.37	285.6	21.21	0.72	4829	16.48	0.83
TiN/CP	Fresh	12.29	279.3	7.58	0.80	76.23	0.584	0.35
	discharged	14.47	573.2	9.34	0.78	72.04	0.526	0.33
	recharged	12.92	422.9	8.37	0.79	154.9	1.03	0.34
TiN@MnO ₂ /CP	Fresh	10.45	173.1	14.52	0.77	25.79	0.20	0.34
	discharged	8.93	355.1	7.32	0.82	31.4	0.04	0.23
	recharged	8.15	223.1	10.07	0.80	47.0	0.92	0.22
TiN@Ir/CP	Fresh	7.31	145.5	16.45	0.76	6.62	0.02	0.37
	discharged	8.82	278.9	13.49	0.78	67.58	0.52	0.35
	recharged	7.46	152	16.45	0.77	29.58	0.26	0.39

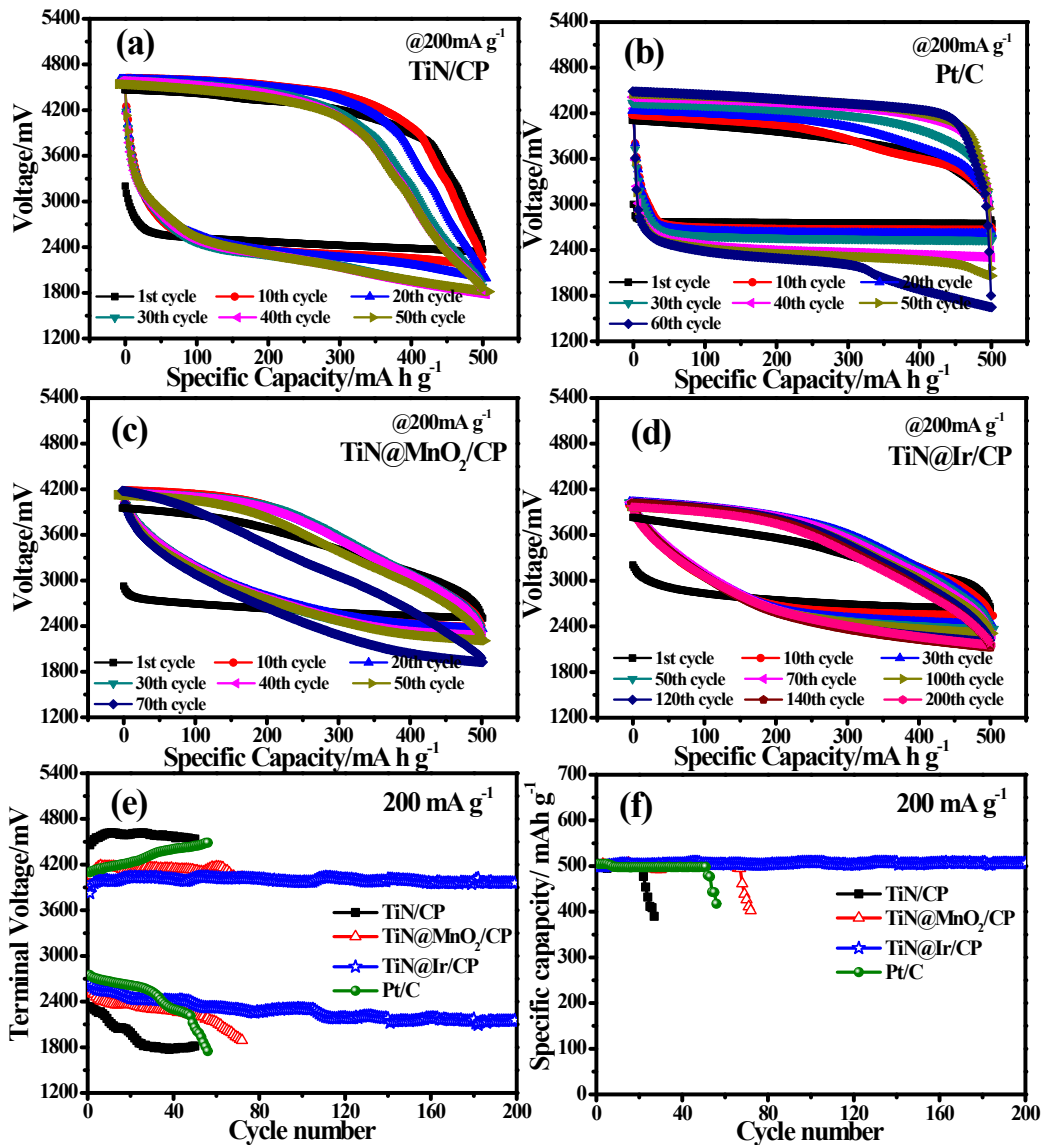


Fig. S11 The cycling performance of Li–O₂ batteries with the (a) TiN/CP, (b) Pt/C, (c) TiN@MnO₂/CP and (d) TiN@Ir/CP electrodes at 200 mA g^{-1} with a limited capacity of 500 mA h g^{-1} ; (e) the terminal voltage and (f) capacities of discharge with various cathodes vs. cycle number.

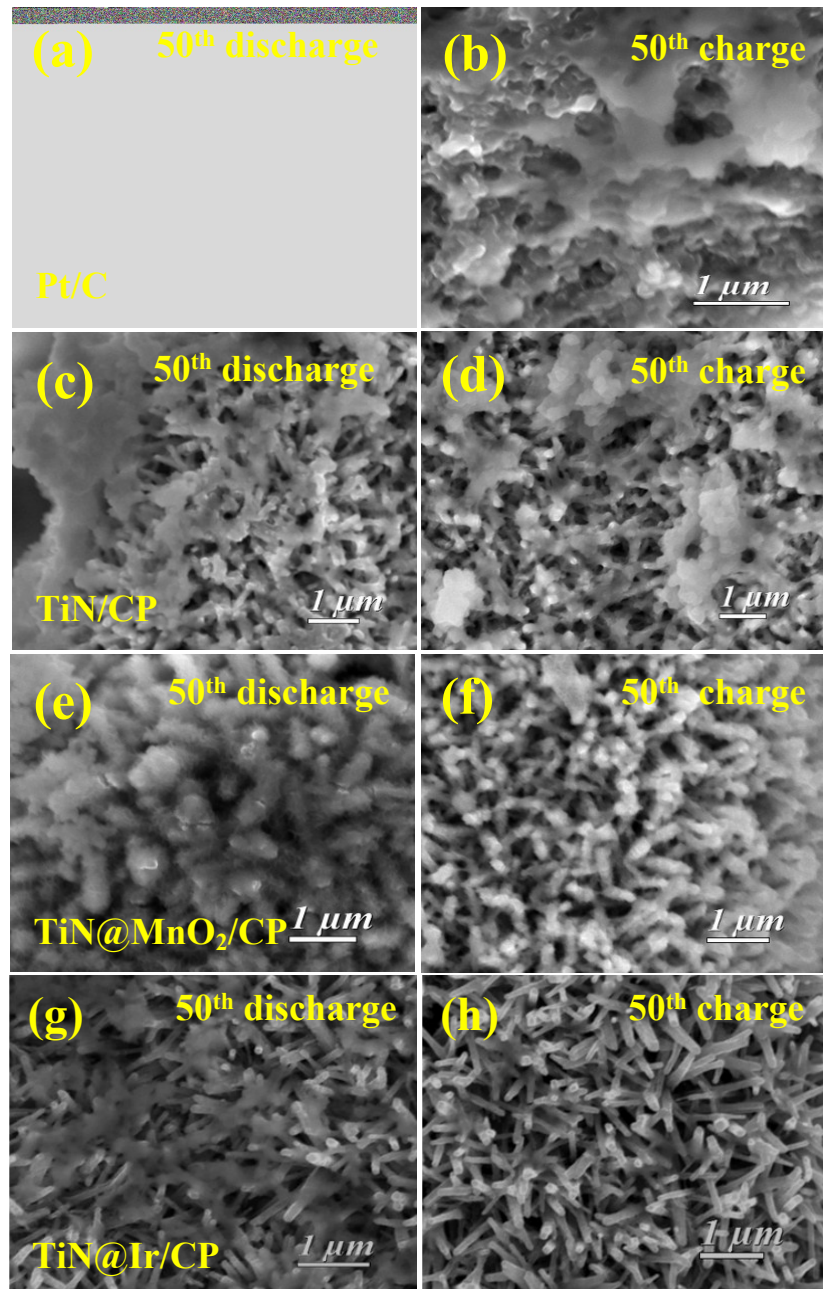


Fig. S12 SEM images of Li–O₂ batteries with the (a, b) Pt/C; (c, d) TiN/CP; (e, f) TiN@MnO₂/CP and (g, h) TiN@Ir/CP cathodes after the 50th discharged (a, c, e, g) and charged (b, d, f, h) at 100 mA g⁻¹ with a fixed capacity of 500 mA h g⁻¹.

References

1. X. C. a. C. Burda, *J. Phys. Chem. B*, 2004, 108, 15446-15449.
2. J. Z. Ye Cong, Feng Chen and Masakazu Anpo, *J. Phys. Chem. C*, 2007, 111, 6976-6982.
3. B. Avasarala, T. Murray, W. Li and P. Haldar, *Journal of Materials Chemistry*, 2009, 19, 1803-1805.
4. T. B. a. D. B. l. Mathieu Toupin, *Chem. Mater.*, 2004, 16, 3184-3190.
5. A. L. Reddy, M. M. Shaijumon, S. R. Gowda and P. M. Ajayan, *Nano letters*, 2009, 9, 1002-1006.
6. M. C. a. M. Ishikawa, *Journal of The Electrochemical Society*, 2000, 147, 2246-2251.